Computational Mechanics
https://doi.org/10.1007/s00466-026-02762-1

ORIGINAL PAPER

Deterministic methodologies for aggregation, breakage, growth and nucleation population balances

Zeeshan Ansari[1] · Mitchell Rae[1] · Nikhil Sriwastav[1,2] · Mainendra Dewangan[2] · Saurabh Tomar[3] · Stefan Heinrich[4] · Rohit Ramachandran[5] · Gavin Walker[2] · Mehakpreet Singh[1,4]

Received: 10 September 2025 / Revised: 8 December 2025 / Accepted: 3 February 2026

Abstract

Population balance equations (PBEs) have previously been applied for modelling across different fields including astrophysics for cloud formation, bubble dynamics, and liquid-liquid dispersion processes. In this paper, a generalised numerical method is presented by enabling the efficient solution of aggregation, breakage, growth, and nucleation mechanisms. A volume-conserving finite volume approximation is developed for the aggregation and breakage processes while the method of characteristics is used for the growth process. This addresses the instability in solutions of combined breakage-growth or aggregation-growth PBEs. Additionally, a nuclei-size cell is introduced at each time step to handle the combined aggregation-nucleation and breakage-nucleation processes. This approach eliminates the need to convert the original aggregation and breakage population balances into divergence form, allowing stable numerical solutions to be obtained for combined processes [Math. Models Methods Appl. Sci. 23(7), 235–1273]. The new numerical approximations are robust for handling complex simultaneous processes, effectively reducing numerical diffusion and dispersion. The accuracy and efficiency of the proposed scheme are validated through comparisons with newly derived analytical results and existing finite volume schemes, fixed pivot technique, and cell average technique, demonstrating its superiority in performance. The comparison shows that the new schemes predict number density functions (NDFs) and their integral moments with significantly higher precision. Computationally, the proposed approach captured all numerical results by consuming 40–70% lesser computational time compared to existing schemes.

Keywords Population balances · Nonlinear integro-partial differential equations · Finite volume schemes · Fixed pivot technique · Cell average technique

Mathematics Subject Classification 35A01 · 35Q70 · 45K05

Zeeshan Ansari and Mehakpreet Singh have contributed equally to this work.

✉ Mehakpreet Singh
Mehakpreet.Singh@ul.ie

Zeeshan Ansari
ansari.zeeshan@ul.ie

Mitchell Rae
rae.mitchell@ul.ie

Nikhil Sriwastav
nikhilsrivastava416908@gmail.com

Mainendra Dewangan
mainendra.dewangan@ul.ie

Saurabh Tomar
sauravtomar9793@gmail.com

Stefan Heinrich
stefan.heinrich@tuhh.de

Rohit Ramachandran
rohit.r@rutgers.edu

Gavin Walker
Gavin.Walker@ul.ie

[1] Mathematics Applications Consortium for Science and Industry (MACSI), Department of Mathematics and Statistics, University of Limerick, Limerick V94T9PX, Ireland

[2] Department of Chemical Sciences, University of Limerick, Limerick V94T9PX, Ireland

[3] Department of Applied Sciences, Rajiv Gandhi National Aviation University, Amethi, UP 229302, India

Published online: 10 March 2026

1 Introduction

Population balance equations (PBEs) are indispensable for tracking the time evolution of particle distributions, serving as a critical framework in engineering and pharmaceutical sciences to address dynamic changes caused by mechanisms such as aggregation (coagulation), breakage (fragmentation), growth, and nucleation. Figure 1 provides a comprehensive visualisation of these mechanisms, illustrating their interrelations across diverse applications. For instance, in slurry fluctuation [1, 2], crystallisation [3, 4], particle size control is vital, while in precipitation processes [5], cheese manufacturing in dairy sciences [6–9] and polymerisation reactions [10], particle distribution directly affects material properties and final product quality. Additionally, pharmaceutical manufacturing involves PBEs to ensure consistent particle size for drug efficacy [11–15]. Such processes influence particle characteristics, including size, volume, and solid–liquid ratios, all of which impact performance outcomes. This evolution is mathematically described by integro-partial differential equations, capturing the complex dependencies within the number density function. Given that real-world distributions may span several magnitudes and exhibit complex peak structures, advanced numerical methods are necessary for accuracy and stability. An efficient numerical solution allows precise modelling, enabling optimal design and control of processes where particle dynamics are central to quality and functionality.

1.1 Mathematical model

In this section, a mathematical model represented by a nonlinear PBE involving aggregation, breakage, growth and nucleation processes is provided. The one-dimensional PBE for a well mixed system used to describe the dynamics of the system [16] can be written as follows

$$\frac{\partial h(t,x)}{\partial t} + \frac{\partial [G(t,x)h(t,x)]}{\partial x} = W^{\pm}_{agg}(t,x) + W^{\pm}_{brk}(t,x) + W_{nuc}(t,x), \tag{1}$$

with initial condition $h(0,x) = h_0(x)$, $x \in \mathbb{R}_+$, where, $(t,x) \in \mathbb{R}^2_+$ and $\mathbb{R}_+ := (0,\infty)$. Further,

- x : represents property of the particle (size or volume).
- $h(t,x)$: represents number density function (NDF).
- $G(t,x)$: growth rate.
- $W_{nuc}(t,x)$: rate at which particles properties x are nucleated.
- $W^{\pm}_{agg}(t,x)$: provides the information of formation of x due to birth and death and is defined as

$$Q^{\pm}_{agg}(t,x) = \frac{1}{2}\int_0^x \alpha(t,x-u,u) f(t,x-u)h(t,u)du - \int_0^\infty \alpha(t,x,u)h(t,x)h(t,u)du. \tag{2}$$

The first expression on RHS of Eq. (2) accounts for the generation of particles x as a result of aggregation of $x-u$ and u. In addition, the second expression on RHS represents the omission of the particles x due to the merging of u and x particles. The aggregation kernel $\alpha(t,x,u)$ describes the interaction (merging) rate of particles x and u. Here $\alpha(t,x,u) \geq 0$ and symmetric in nature $\alpha(t,x,u) = \alpha(t,u,x)$.

- $W^{\pm}_{brk}(t,x)$: describes the formation of particles x due to linear fragmentation process and is defined by

$$W^{\pm}_{brk}(t,x) = \int_x^\infty \mathcal{B}(x,u)F(u)h(t,u)du - F(x)h(t,x). \tag{3}$$

here $\mathcal{B}(x,u)$ denotes the distribution of particles x formed from u. Here the function $\mathcal{B}(x,u)$ must follows:

(a) $\int_0^x \mathcal{B}(x,u)du = \nu(x) \geq 2$, where $\nu(x)$ defines the number of daughter particles due to breakage of mother particle u, and

(b) $\int_0^u x\mathcal{B}(x,u)du = u$, shows the conservation of total volume between the daughter particle x and mother particle u.

In addition, $F(x)$ represents the selection rate of particle x that undergo break and can be expressed mathematically as $F(x) = F_0F^*(x)$ where F_0 is considered to be 1 for the simple cases.

Some recent semi-analytical methods for PBEs are given in [17–27] and references therein. These approaches require a large number of series terms to accurately capture system dynamics over extended time frames, resulting in high computational costs and limiting their practicality for real-life applications. This issue can be addressed with numerical methods including finite volume schemes (FVS) [28–35], quadrature method of moments [36–40], fixed pivot technique (FPT) [41–45], stochastic methods [46–51] and cell average technique (CAT) [52]. Some other numerical methods for solving aggregation and breakage PBEs can be found

[4] Bernal Institute, University of Limerick, Limerick V94T9PX, Ireland

[5] Chemical and Biochemical Engineering, Rutgers University, 98 Brett Road, Piscataway, NJ 08854, USA

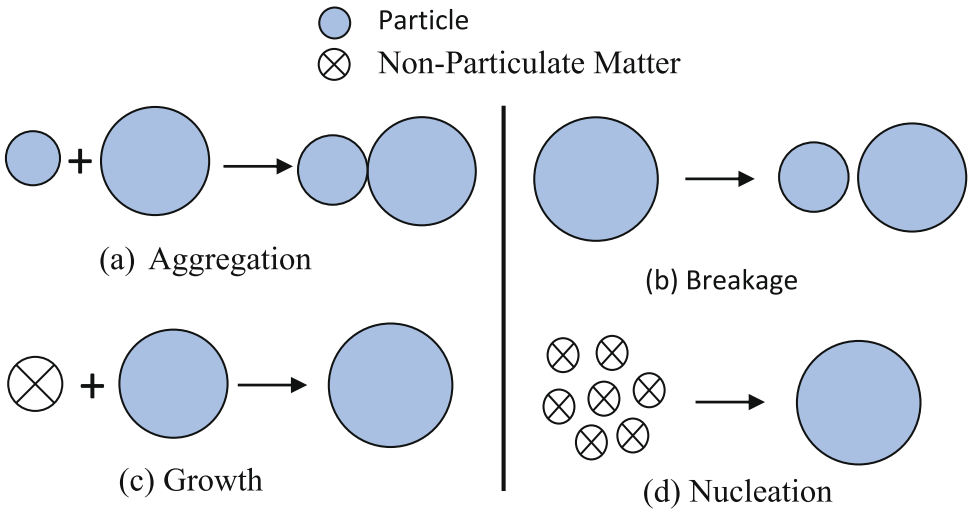

Fig. 1 Various particles formation mechanisms

in [53–57]. To the best of our knowledge, there has been no comprehensive critical review in the existing literature that thoroughly examines simultaneous solutions to the PBEs. This gap highlights the need for a detailed and systematic analysis of such approaches to better understand their theoretical foundations, computational strategies, and practical implications.

In the work described in [58], the aggregation process is addressed using the FPT. However, this approach introduces numerical diffusion due to the distribution of the particle properties to the neighbouring nodes, which hinders the accurate estimation of the NDF for the larger size particles. The issue of numerical diffusion was further tackled using method of characteristics for the coupled aggregation-growth PBEs [41]. Whereas, the CAT is highly accurate but has a major drawback related to its complex mathematical formulation and tends to be computationally expensive. The numerical methods presented by [29] offer simpler formulations compared to previous approaches. However, these methods require the conversion of the original PBE into the conservative form to achieve stable solutions and loss the information of the NDFs. In addition, the finite volume scheme [31], reformulates the CAT into a conservative form. Nonetheless, the main drawback of this method lies in its complex formulation, resulting in significant CPU time requirements for tracking important results. A comprehensive discussion regarding the merits and disadvantages of the sectional methods and finite volume schemes for pure aggregation PBE is provided in the referenced literature [59] and also discussed in detail in Sect. 3. Recently, Hong et al. [60] and Zhang et al. [61] introduced an improved high-resolution algorithm for solving growth and nucleation PBEs. Furthermore, discretized formulations based on finite difference methods have been proposed for one and two-dimensional growth and nucleation PBEs [62, 63]. Nevertheless, these methodologies warrant further investigation to facilitate their application to aggregation, breakage, and coupled PBEs.

The current study has two main objectives. First, we propose a generalised numerical scheme that offers a straightforward formulation, ease of coding, and the ability to accurately predict various order moments and the NDF with higher precision. Notably, this new scheme does not require any conversion of the original PBE into the mass conservative form to obtain stable solutions for coupled systems. Second, a comprehensive qualitative and quantitative comparison is performed between the proposed method and existing approaches, including FPT [58], CAT [52], and FVSs [29, 64]. The merits and limitations of each method are critically examined to provide valuable insights into the robustness of the schemes in capturing the desired results. Through this analysis, the strengths and weaknesses of the FPT, CAT, and the proposed FVSs are thoroughly evaluated, highlighting a promising direction toward developing unified, efficient, and accurate frameworks for solving and optimizing a wide range of particulate processes.

This article is arranged as follows: Sect. 2, the mathematical formulation of the new schemes are provided to solve combined processes problems along with the description of the grid discretisation. Further, In Sect. 3, we validate the accuracy and efficiency of the newly proposed schemes. In Sect. 4, the conclusion and remarks of the current study is made.

2 Numerical methods

In this part of the paper we formulate the mathematical expression of the numerical approximations for Eq. (1). The main hypothesis considered to derive the numerical methods is that the particles within a each cells are available only on its representatives (pivot or centre). Let us now provide the

information of t discretisation domain require for developing the numerical methods. We divide the continuous domain $[0, x_{max} < \infty]$ into I number of sub-cells having x_i as centre volume, for $i \in 1, 2, ..., I$ (see Fig. 2). Now, define the pivots and the cell size by

$$x_{1/2}=0, \quad x_i=\frac{x_{i-1/2}+x_{i+1/2}}{2}, \quad \Delta x_i = x_{i+1/2} - x_{i-1/2}.$$

Since the numerical discretisation is employed to solve the PBE represented by Eq. (1), the infinite integral makes it challenging to solve with numerical approaches. Therefore, to develop numerical schemes, it is necessary to restrict the discretised domain to a finite region $\omega := \{(x, u) : 0 < x < x_{max}, 0 < u < u_{max}\}$ and the aggregation kernel is restricted to:

$$\alpha(t, x, u) = \begin{cases} \alpha(t, x, u), & (x + u) \leq x_{max}; \\ 0, & \text{otherwise.} \end{cases} \tag{4}$$

Note: While running the numerical simulations, no restrictions have been imposed on the the aggregation kernel.

2.1 Pure aggregation

The mathematical derivation of the FVS for solving pure aggregation PBE is provided for a non-uniform grid. By substituting the value of the $S_0, G, Q = 0$ in the original PBE (Eq. 1), the pure aggregation can be obtained. For the description of the formulation, it is required to define the following set:

$$S^i = \left\{(j, k) \in \mathbb{N} \times \mathbb{N} : x_{i-1/2} < (x_j + x_k) \leq x_{i+1/2}\right\} \tag{5}$$

where lower $(x_{i-1/2})$ and upper $x_{i+1/2}$ boundaries of the ith cell. and the x_i is the centre of the ith cell (as shown in Fig. 2). Graphically the set S^i is demonstrated in Fig. 3.

Furthermore, discretise the time domain into discrete time intervals represented as $t^{n+1} = t^n + \Delta t^n$, where $n \in \mathbb{N}$. Additionally, consider a function h_i^n, denoting the mean value of h at time t^n within the ith cell, where $i \in 1, 2, \ldots, I$. This average value is equivalent to $h(t^n, x_i)$ and can be defined as:

$$h_i^n = \frac{1}{\Delta x_i} \int_{x_{i-1/2}}^{x_{i+1/2}} h(t^n, x) dx. \tag{6}$$

The main concept of the scheme is to approximate the integrals in Eq. (1) by assuming that the volumes of particles are only available on pivots of discretised domain. This mathematical description can be further elucidated as follows:

$$h(t, x) \approx \sum_{j=1}^{I} h_j \Delta x_j \delta(x - x_j). \tag{7}$$

Using the above expression of $f(t, x)$ in Eq. (1) and we define the finite volume scheme as

$$\frac{dh_i}{dt} = \frac{1}{2} \sum_{(j,k)\in S^i} \alpha(x_j, x_k) h_j h_k \frac{\Delta x_j \Delta x_k}{\Delta x_i} - \sum_{j=1}^{I} \alpha(x_i, x_j)\, h_i h_j \Delta x_j. \tag{8}$$

The essential criteria for the finite volume scheme is to conserve the system properties such as volume, mass or number. However, the formulation (Eq. 8) does not hold the volume conservative property. Therefore, adding extra correction factor to the birth term is done for fulfilling this criteria. Finally we arrive at

$$\frac{dh_i}{dt} = \frac{1}{2} \sum_{(j,k)\in S^i} \alpha(x_j, x_k) h_j h_k \frac{\Delta x_j \Delta x_k}{\Delta x_i}\, \Omega_{i,j,k} - \sum_{j=1}^{I} \alpha(x_i, x_j) h_i h_j \Delta x_j. \tag{9}$$

Discretising the time derivative using the first order Euler method, we get

$$h_i^{n+1} = h_i^n + \Delta t^n \Bigg(\underbrace{\frac{1}{2} \sum_{(j,k)\in S^i} \alpha(x_j, x_k) h_j^n h_k^n \frac{\Delta x_j \Delta x_k}{\Delta x_i}\, \Omega_{i,j,k}}_{:=B_{agg,i}^{\text{FVS}}} - \underbrace{\sum_{j=1}^{I} \alpha_{i,j}^n h_i^n h_j^n \Delta x_j}_{:=D_{agg,i}^{\text{FVS}}} \Bigg), \tag{10}$$

where $\Omega_{i,j,k}$ ensures total volume conservation and expressed mathematically as

$$\Omega_{i,j,k} = \begin{cases} \dfrac{x_j + x_k}{x_i}, & x_j + x_k \neq x_i; \\ 1, & x_j + x_k = x_i; \\ 0, & x_j + x_k < 0 \text{ or } x_j + x_k > x_{max}. \end{cases} \tag{11}$$

It can be noted that the correction factor $\Omega_{i,j,k}$ is responsible for the conservation of total volume. It can be noted that the FVS scheme is developed with the purpose of conserving one property of the system, that is, total volume. A detailed explanation of FVS scheme and theoretically proof of the conservation of total volume in the system can be found in [65]. It is important to note that incorporating this weight adversely affects the zeroth-order moment, that is, not conserved.

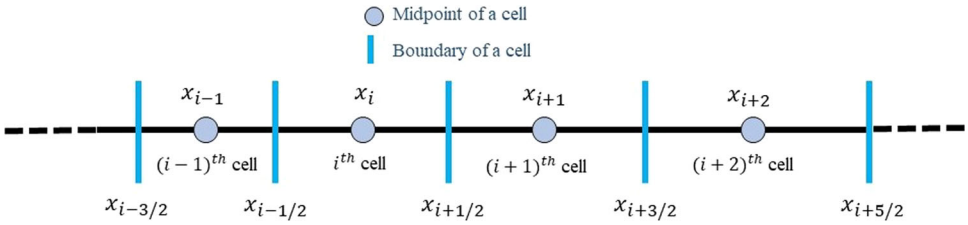

Fig. 2 Discretised domain for numerical methods

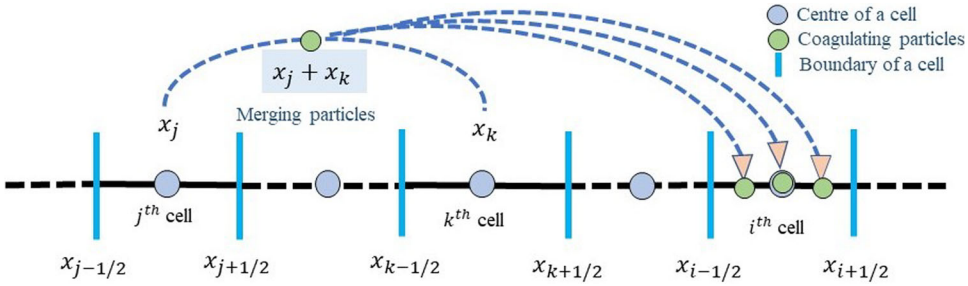

Fig. 3 Representation of set S^i

2.2 Pure breakage

In this section, we will outline the formulation of the finite volume scheme developed by [66] for solving pure breakage PBE. A pure breakage PBE can be derived from the Eq. (1) by setting α_0, G, and W equal to zero. The idea of this scheme is similar to the previous case, that is, to conserve the total volume in the system.

Using the set defined in Eq. (5) and the same discretisation domain, the final set of ODEs of the FVS for the pure breakage PBE are written as follows:

$$\frac{dh_i}{dt} = \frac{1}{\Delta x_i}\sum_{k=i}^{I} F_k h_k \Delta x_k \int_{x_{i-1/2}}^{p_k^i} \mathcal{B}(x, x_k)dx - \beta_i F_i h_i. \tag{12}$$

Like previous case, discretise the time derivative present on the LHS using the first order Euler method, the above equation changes to

$$f_i^{n+1} = h_i^n + \Delta t^n \Big(\underbrace{\frac{1}{\Delta x_i}\sum_{k=i}^{I} F_k h_k^n \Delta x_k \int_{x_{i-1/2}}^{p_k^i} \mathcal{B}(x, x_k)dx}_{:=B_{break,i}^{\text{FVS}}} - \underbrace{\beta_i F_i h_i^n}_{:=D_{break,i}^{\text{FVS}}} \Big), \tag{13}$$

where β_i is the weight factor that ensures the total volume conservation and is defined as

$$\beta_i = \frac{1}{x_i}\sum_{k=1}^{i} x_k \int_{x_{k-1/2}}^{p_i^k} \mathcal{B}(x, x_i)dx, \; i = 1, 2, \cdots, I, \tag{14}$$

where

$$p_k^i = \begin{cases} x_i, & \text{if } k = i, \\ x_{i+1/2}, & \text{if } k \neq i. \end{cases}$$

It can be easily noticed that the formulation (Eq. 13) is not holding the volume conservation property without the weight factor β_i. This means the correction factor ensures that the total volume is conserved at each time step. The detailed description of the FVS and proof of the volume conservation law can be found in [66].

2.3 Simultaneous aggregation and breakage (SAB)

Now the numerical formulation of the FVS for a SAB PBE is provided. The required equation can be obtained from the original equation by setting up the parameters $G, Q = 0$. Conventionally, the numerical approximation of the simultaneous aggregation and breakage processes is done by the addition of individual birth and death terms. Thus the expression takes the following form:

$$\frac{dh_i}{dt} = \frac{1}{2}\sum_{(j,k)\in S^i} \alpha(x_j, x_k) h_j^n h_k^n \frac{\Delta x_j \Delta x_k}{\Delta x_i}\, \Omega_{i,j,k} - \sum_{j=1}^{I} \alpha_{i,j}^n h_i^n h_j^n \Delta x_j \tag{15}$$

$$+ \frac{1}{\Delta x_i}\sum_{k=i}^{I} F_k h_k^n \Delta x_k \int_{x_{i-1/2}}^{p_k^i} \mathcal{B}(x, x_k)dx - \beta_i F_i h_i^n. \tag{16}$$

This formulation holds the volume conservation as the both individual formulations hold this conservation property. The theoretical proof of volume conservation law is provided in [67]. To efficiently solve these simultaneous processes, we

consider the combined birth and death rates from both aggregation and breakage. In this approach, all particles entering a given cell–regardless of whether they arise from aggregation or breakage–are collectively accounted for. Then final expression for the simultaneous aggregation-breakage PBE can be written as

$$\frac{dh_i}{dt} = \frac{1}{2}\sum_{(j,k)\in S^i} \alpha(x_j, x_k) h_j^n h_k^n \frac{\Delta x_j \Delta x_k}{\Delta x_i}\, \Omega_{i,j,k} + \frac{1}{\Delta x_i}\sum_{k=i}^{I} F_k h_k^n \Delta x_k \int_{x_{i-1/2}}^{p_k^i} \mathcal{B}(x, x_k) dx - \sum_{j=1}^{I} \alpha_{i,j}^n h_i^n h_j^n \Delta x_j - \beta_i F_i h_i^n. \tag{17}$$

where the first-two terms on RHS of equation represents the birth (formation) of the particles in the ith cell due to both aggregation and breakage processes. Similarly, the last-two terms of the RHS show the death (omission) of the particles in the ith cell due to both processes.

Remark The techniques provided in Sects. 2.1, 2.2 and 2.3 are only focused on tracking the total volume in the system accurately. Nevertheless, no efforts were made to conserve the total number of particle (zeroth order moment). Nonetheless, it would be interesting to evaluate how effectively these methods can represent the zeroth-order moment.

2.4 Simultaneous aggregation/breakage and growth

Now the numerical approximation for the simultaneous growth and aggregation/breakage (SGA/B) processes are derived. Previously, Kumar [68] have implemented the CAT to solve SGA problem. The primary limitation of this method was its inability to accurately predict moments of different orders. Later, Qamar [69] formulated a FVS with a method of characteristic (MOC) to solved this problem. But, the number distribution function shows large deviation compared to the exact solutions. Additionally, implementing this method required reformulating the original PBE into a volume-conservative form to stabilize the solution. The inability of the existing FVS to effectively couple with the MOC motivated us to develop a more accurate approach for simultaneously handling aggregation/breakage, and growth, while also reducing CPU time. Previous studies have demonstrated that the growth process can be treated similarly to breakage (alongside aggregation), though numerical diffusion poses a significant challenge [68]. Consequently, the moving pivot method is generally considered the most effective technique for addressing the growth problem.

Our proposed approach involves utilizing the FVS to approximate the aggregation and breakage problems, as discussed in Sects. 2.1 and 2.2, respectively. On the other hand, a Lagrangian approach can be adopted specifically for handling the growth process, aiming to achieve more accurate numerical results. The resulting set of ODEs formed for solving the SGA/B problems can be expressed as:

$$\frac{dh_i}{dt} = \frac{1}{2}\sum_{(j,k)\in S^i} \alpha(x_j, x_k) h_j^n h_k^n \frac{\Delta x_j \Delta x_k}{\Delta x_i}\, \Omega_{i,j,k} - \sum_{j=1}^{I} \alpha_{i,j}^n h_i^n h_j^n \Delta x_j, \tag{18}$$

and

$$\frac{dh_i}{dt} = \frac{1}{\Delta x_i}\sum_{k=i}^{I} F_k h_k^n \Delta x_k \int_{x_{i-1/2}}^{p_k^i} \mathcal{B}(x, x_k) dx - \omega_i F_i h_i^n, \tag{19}$$

together with

$$\frac{dx_i}{dt} = G(x_i), \tag{20}$$

and

$$\frac{dx_{i+1/2}}{dt} = G(x_{i+1/2}). \tag{21}$$

In the aforementioned Eqs. (18) and (19) represent the evolution of particles properties with time due to the aggregation and breakage process, respectively. On the other hand, Eqs. (20) and (21) describe the changes in the mean and boundaries of the ith cell, respectively. It is worth noting that we have considered only time independent growth kernels for our study.

Additionally, for solving the combined aggregation-brea kage-growth problem, the FVS for solving the aggregation and breakage processes remains the same as described in Sect. 2.3. Once again, a Lagrangian approach can be employed for the growth process. Consequently, the final set of ODEs formed for the combined aggregation and breakage can be described as follows

$$\frac{dh_i}{dt} = \frac{1}{2}\sum_{(j,k)\in S^i} \alpha(x_j, x_k) h_j^n h_k^n \frac{\Delta x_j \Delta x_k}{\Delta x_i}\, \Omega_{i,j,k} + \frac{1}{\Delta x_i}\sum_{k=i}^{I} S_k f_k^n \Delta x_k \int_{x_{i-1/2}}^{p_k^i} \mathcal{B}(x, x_k) dx - \sum_{j=1}^{I} \alpha_{i,j}^n h_i^n h_j^n \Delta x_j - \omega_i S_i f_i^n. \tag{22}$$

and for solving the growth process, the Eqs. (20) and (21) can be implemented.

2.5 Simultaneous aggregation/breakage and nucleation

In this section, we focus on solving simultaneous aggregati on-nucleation PBE and breakage-nucleation PBE through numerical methods. When it comes to handling nucleation, there are two possible approaches:

(a) If the nucleation is assumed to be mono-disperse, a boundary condition can be set near the lower boundary of the first cell (closer to size zero).
(b) An alternate approach is to place a source located near the lower boundary of the first cell.

For our study, we opted the second possibility to handle the nucleation process.

The standard formulation for combining the aggregation-nucleation mechanism (Eq. 23) with the breakage-nucleation mechanism (Eq. 24) is expressed as

$$\frac{dh_i}{dt} = \frac{1}{2}\sum_{(j,k)\in S^i} \alpha(x_j, x_k) h_j^n h_k^n \frac{\Delta x_j \Delta x_k}{\Delta x_i}\, \Omega_{i,j,k} - \sum_{j=1}^{I} \alpha_{i,j}^n h_i^n h_j^n \Delta x_j + \int_{x_{i-1/2}}^{x_{i+1/2}} B_{nuc}(t,x)dx, \tag{23}$$

and

$$\frac{dh_i}{dt} = \frac{1}{\Delta x_i}\sum_{k=i}^{I} F_k h_k^n \Delta x_k \int_{x_{i-1/2}}^{p_k^i} \mathcal{B}(x, x_k)dx - \beta_i F_i h_i^n + \int_{x_{i-1/2}}^{x_{i+1/2}} B_{nuc}(t,x)dx. \tag{24}$$

However, this formulation has a significant drawback in that it may experience volume loss or gain since it assumes that nucleation occurs exactly at the representative of the cell. In reality, it is rare for particles to fall exactly on the representative of the cell after nucleation, which can lead to instability in the solution. To address this limitation, Kumar et al. [68] proposed the CAT, offering a more efficient approach to coupling the aggregation-nucleation and breakage-nucleation processes. However, the CAT can be computationally demanding due to the added overhead of averaging particle volumes and redistributing these average values to neighbouring pivots. Additionally, numerical diffusion can occur during the reassigning of particle properties to the neighbouring pivots, further impacting the accuracy of the solution.

The FVS for coupling the aggregation-nucleation and breakage-nucleation processes is represented by

$$\frac{dh_i}{dt} = B^{\text{FVS}}_{agg+nuc,i}/B^{\text{FVS}}_{break+nuc,i} - D^{\text{FVS}}_{agg,i}/D^{\text{FVS}}_{break,i}. \tag{25}$$

Here $B^{\text{FVS}}_{agg+nuc,i}$ denotes the addition of the birth terms of aggregation and nucleation process, whereas $B^{\text{FVS}}_{break+nuc,i}$ represents the sum of the birth terms of breakage and nucleation process. It is important to note that the formulation may result in minor mass discrepancies if nucleation occurs away from the representative sizes, x_i. To preserve moment consistency in the fixed pivot framework, the generated particles are accordingly redistributed among adjacent cells. While a detailed examination of this issue is not pursued here, we proceed to outline the treatment of such problems within the framework of the finite volume scheme.

It is known that the nucleation process always leads to the birth of particles and does not involve the death of particles. Moreover $D^{\text{FVS}}_{agg,i}$ and $D^{\text{FVS}}_{break,i}$ denote the death terms of the aggregation and breakage process. Equation (25) provides a framework applicable to the solution of general polydisperse nucleation problems. However, for a mono-disperse nucleation scenario, the appearance of the smallest size particle and the smallest mean of the cell is considered in a way that matches with the appearance of the mono-disperse particles (for more detail, refer to [68]). As a result, the above expression is changed to

$$\frac{df_1}{dt} = B^{\text{FVS}}_{agg,1}/B^{\text{FVS}}_{break,1} - D^{\text{FVS}}_{agg,i}/D^{\text{FVS}}_{break,1} + B_{nuc}(t, x_1), \tag{26}$$

and

$$\frac{dh_i}{dt} = B^{\text{FVS}}_{agg,i}/B^{\text{FVS}}_{break,i} - D^{\text{FVS}}_{agg,i}/D^{\text{FVS}}_{break,i}, \quad \text{for } i = 2, 3, \cdots, I. \tag{27}$$

Important Note: The simultaneous aggregation-breakage-nucleation PBE can be approximated using the following discretization:

$$\frac{dh_i}{dt} = B^{\text{FVS}}_{agg+break+nuc,i} - D^{\text{FVS}}_{agg+break,i}, \tag{28}$$

where

$$B^{\text{FVS}}_{agg+break+nuc,i} = B^{\text{FVS}}_{agg+break,i} + \int_{x_{i-1/2}}^{x_{i+1/2}} B_{nuc}(t,x)dx. \tag{29}$$

3 Numerical results and discussions

In this section, we seek to validate the accuracy of the newly developed numerical schemes (NFVS) by comparing them against the existing finite volume schemes [29, 64], the fixed pivot technique [58] and the cell average technique (CAT) [52]. The comparison of results is done by comparing the NDF and first two moments. The moments are non-dimensionalized by dividing them by their respective initial values. The integral moments corresponding to $h(t, x)$ are of great interest and can be estimated using the formula

$$\mu_i(t) = \int_0^\infty x^i h(t, x) dx, \tag{30}$$

for integers $i = 0, 1, 2, \ldots$. Here $(\mu_0(t))$ and $(\mu_1(t))$ zeroth and the first order moments, respectively. To show the accuracy of numerical methods, the quantitative relative errors in the different order moments are calculated using

$$\Delta_i(t) = \left| \frac{\mu_i^{ana} - \mu_i^{num}}{\mu_i^{num}} \right|. \tag{31}$$

here *ana* and *num* represent the solution obtained analytically (exact) and numerically, respectively.

For this work, numerical calculations were done using `ode45` solver in `MATLAB` on a computer with specifications `i7` CPU (2.80 `GHz`) and 16 `GB RAM` with both relative and absolute error tolerances are considered to be 10^{-6}. It is worth mentioning that all the results are obtained for dimensionless volume and time. For all comparisons, $f(0, x) = \exp(-x)$ is considered.

3.1 Results for pure aggregation

We first compare the numerical results obtained using different numerical methods including exiting finite volume scheme (FVS-2004), fixed pivot technique (FPT) and the cell average technique (CAT) [52, 58, 64] for the constant kernel $(\alpha(x, u) = 1)$. For the comparison, the moments of different orders and the number density function computed by all numerical schemes are evaluated against the exact results. A quantitative error analysis is performed to estimate the errors in the zeroth, first, and second-order moments. The domain $[10^{-6}, 10^3]$ is divided into 50 non-uniform cells, and simulations are run until $t = 18$. The comparisons of NDF and their moments is shown in Fig. 4.

It can be seen from Fig. 4a that the zeroth-order moment (ZOM) is qualitatively well predicted by all numerical methods. Moreover, the first-order moment (FOM) shown in Fig. 4b is accurately captured by the proposed approach and CAT, whereas the existing FVS and FPT methods exhibit a small loss of volume from the system. In addition, the second order moment is significantly more accurately estimated by the CAT and proposed approach than the existing FVS and FPT methods (refer to Fig. 4c). Although slight deviations exist among the results, these differences are difficult to identify qualitatively. Therefore, an error analysis is performed by estimating the quantitative relative errors in the moments for 30 and 50 non-uniform cells, as presented in Table 1. It can be observed from the table that the proposed approach demonstrates higher accuracy compared to the other numerical methods. It is also worth noting that no specific measures were taken to enhance the accuracy of the zeroth- and second-order moments in case of the proposed approach.

Table 1 Quantitative comparison of errors for all methods and their respective computational time

Cells	Technique	Δ_0	Δ_1	Δ_2	CPU
30	FPT	0.6330	3.7755×10^{-8}	1.2291	0.1048
	FVS	0.6396	3.8747×10^{-14}	0.9767	0.1309
	CAT	0.6330	2.2204×10^{-16}	0.8138	0.0496
	NFVS	0.6312	0	0.9356	0.0397
60	FPT	0.6330	1.2597×10^{-12}	0.9708	0.1345
	FVS	0.6352	4.4409×10^{-16}	0.8760	0.3025
	CAT	0.6330	6.6613×10^{-16}	0.7950	0.0896
	NFVS	0.6281	2.2204×10^{-16}	0.7988	0.0767

3.2 Results for simultaneous aggregation and breakage (SAB)

Let us now conduct a comparison for checking the accuracy of the NFVS with the CAT [52] for a SAB PBE by considering a product aggregation kernel $(\alpha(x, u) = xu)$ with binary breakage kernel $\mathcal{B}(x, u) = \frac{2}{u}$ and linear selection function $F(x) = x$. The computational domain in the range $[10^{-6}, 10^3]$ is discretised into 50 non-uniform cells, and all simulations are carried out up to time $t = 0.45$.

We compared qualitatively NDF and moments for a SAB PBE in Fig. 5. The ZOM is captured more accurately by the NFVS than CAT. Both methods comply with the volume conservation law, as depicted in Fig. 5a , that is, the FOM is not changed throughout the simulation. Since the results of the analytical NDF is not available for this case, only numerical results are shown in Fig. 5b . It is important to highlight that the CAT method is primarily designed to accurately preserve the first two moments of the NDF. However, its accuracy can be further enhanced by employing a finer computational grid, enabling better resolution of the distribution and capturing more detailed system behavior. In comparison, although the NFVS method focuses solely on ensuring conserving total volume, it demonstrates superior performance in estimating the ZOM relative to CAT. This

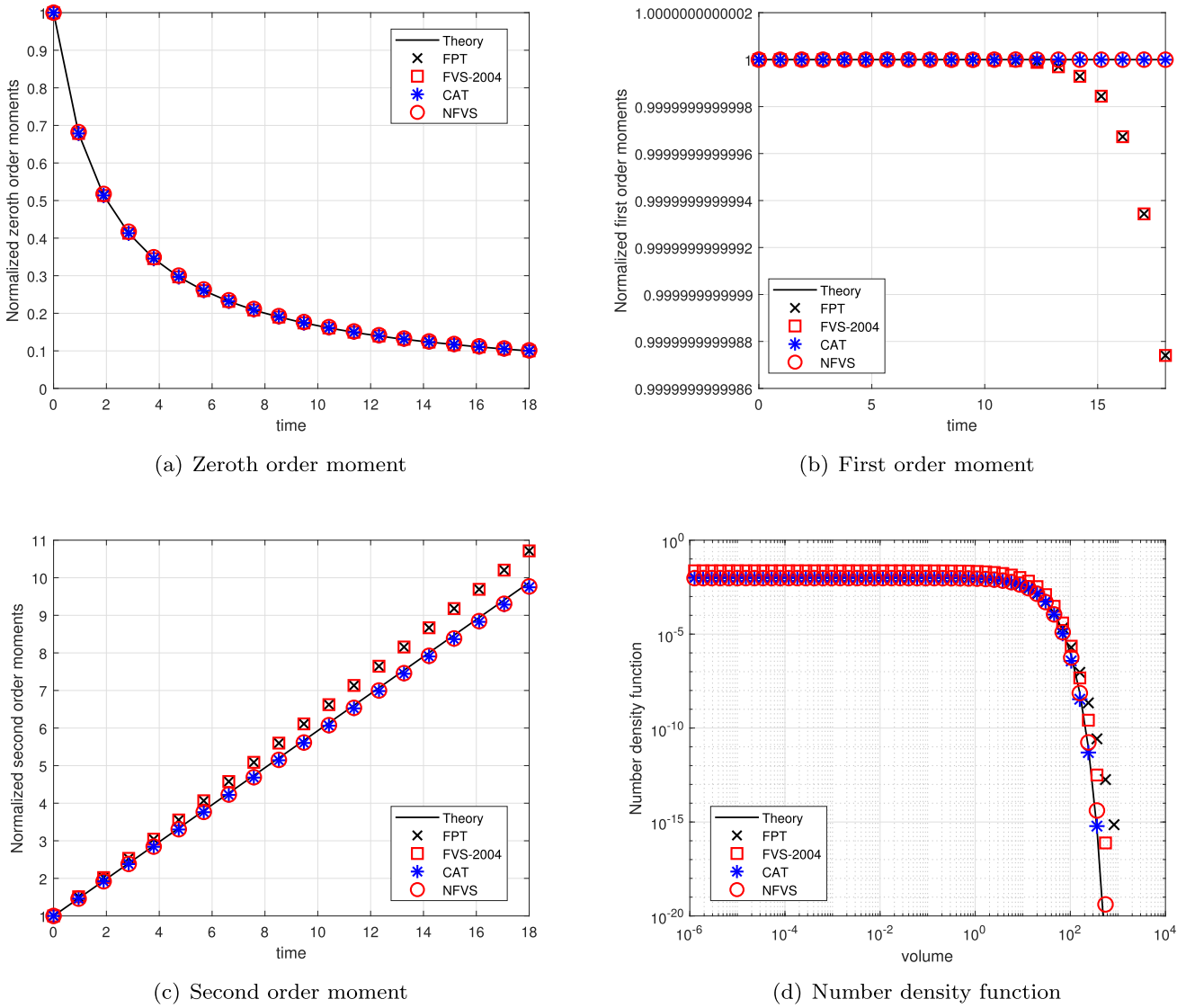

(a) Zeroth order moment

(b) First order moment

(c) Second order moment

(d) Number density function

Fig. 4 Testing of NFVS, FPT, FVS-2004 and CAT in terms of number density and moments for pure aggregation PBE **a** zeroth order moment, **b** first order moment, **c** second order moment, and **d** number density function

advantage arises because CAT introduces numerical diffusion when redistributing particle properties to neighbouring nodes to maintain the first two moments. In contrast, NFVS avoids such redistribution, which contributes to its improved accuracy in preserving the zeroth moment and overall results.

The quantitative relative errors in the ZOM and FOM are calculated using Eq. (31) for different grids and listed in Table 2. The NFVS estimated these results with high precision compared to the EFVS.

Important note: In the next sections, we will compare all numerical results with the existing finite volume scheme (EFVS) [29] in order to enhance the comparison.

Table 2 Quantitative comparison of errors in moments for SAB PBE

Δ	CAT 30 cells	NFVS 30 cells	CAT 60 cells	NFVS 60 cells
Δ_0	0.09593	0.04408	0.10571	0.07415
Δ_1	0.11568	0.00328	0.00165	3.6×10^{-8}

3.3 Simultaneous aggregation-growth (SAG)

We now compare the numerical results computed for the SAG PBE. Two cases are considered:

Case 1: Constant kernel ($\alpha(x, u) = 1$) with linear growth ($G(x) = G_0 x$).

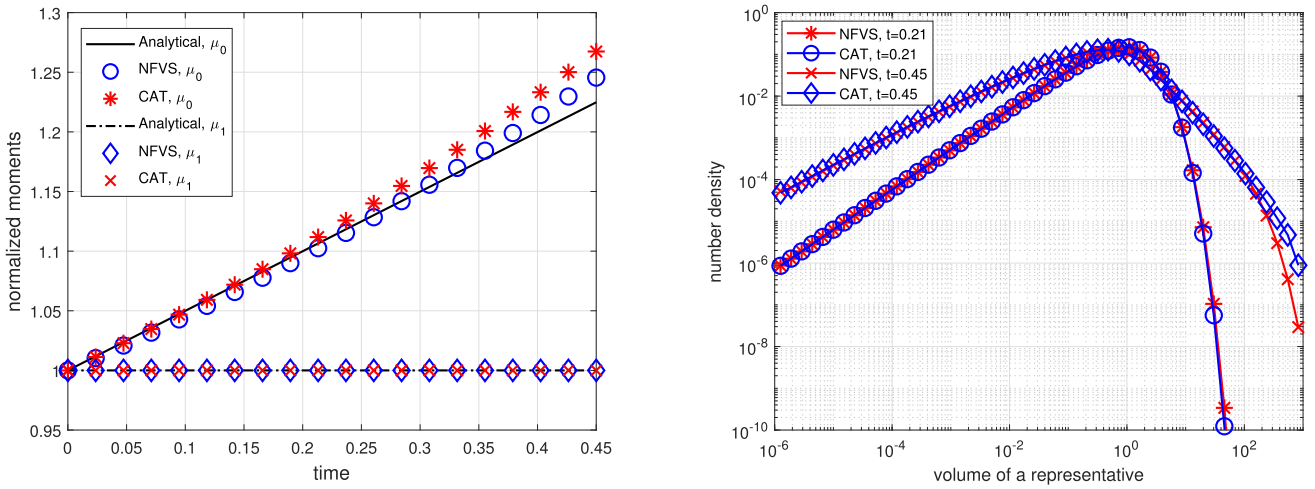

(a) Zeroth and first order moments

(b) Number density function

Fig. 5 Testing of NFVS and CAT of number density and moments for SAB PBE **a** zeroth order moment, and **b** first order moment

Case 2: Sum kernel ($\alpha(x,u) = x + u$) with linear growth ($G(x) = G_0 x$).

The analytical or exact solutions of the NDFs were derived by Hu et al. [70] for both cases.

3.3.1 Case 1

Consider constant aggregation kernel $\alpha(x,u) = 1$ with linear growth function $G(x) = G_0 x$ where $G_0 = 0.10$. The computational grid in the range [10^{-6} 300] is partitioned non-uniformly into 30 cells. The simulations are run till time $t = 30$.

The graphical comparison of the moments and distribution functions is presented in Fig. 6. It is evident that the ZOM estimated by the proposed NFVS method shows highly accurate results, closely matching the exact solution. Whereas, the existing EFVS method exhibits deviation from the reference (exact) solution, as shown in Fig. 6a . The FOMs are equally well captured by both numerical methods, as depicted in Fig. 6b . Furthermore, the NDF calculated by the NFVS match well with the exact NDF, while the EFVS method shows an over-prediction of this result, as seen in Fig. 6c .The resolution of the EFVS can be improved by adding extra non-uniform cells in the computational discretised grid, but this comes at the expense of higher computational cost. The relative errors in first two order moments are estimated for different number of cells and listed in Table 3. The results demonstrate that the NFVS perform better than EFVS. In terms of computational time, CPU times for both methods with different grids is listed in Table 4. Once again, the NFVS outperforms the EFVS, requiring less computational time to estimate the results.

Table 3 Quantitative comparison of errors in moments for Case 1

Δ	EFVS 30 cells	NFVS 30 cells	EFVS 60 cells	NFVS 60 cells
Δ_0	0.2831	0.0200	0.1967	0.0015
Δ_1	1.02×10^{-7}	1.02×10^{-7}	3.02×10^{-9}	1.79×10^{-9}

3.3.2 Case 2

Let us now consider a sum aggregation kernel $\alpha(x,u) = 1$ with linear growth function $G(x) = G_0 x$ where $G_0 = 0.10$. The computational grid [10^{-6} 10^4] is subdivided into 30 non-uniform cells and both simulations are run till time $t = 2.5$.

The NDFs and moments are plotted in Fig. 7, providing a comparison between the NFVS and EFVS methods. The results demonstrate that the ZOM calculated by the NFVS method closely matches the exact moment, while the EFVS method exhibits significant deviation from the exact result as shown in Fig. 7a. Once again, both methods accurately capture the FOM (refer to Fig. 7b). Furthermore, the NFVS method accurately calculated the NDF, while the EFVS method shows considerable deviations from the exact results as demonstrated in Fig. 7c. In terms of CPU time, the NFVS method outperforms the EFVS method, consuming 30% lesser CPU time to run the NFVS simulation as shown in Table 4.

3.4 Simultaneous breakage-growth (SBG)

Let us now test the results obtained from the new approach for solving a SBG PBE. In this test, we consider a binary breakage kernel given by $\mathcal{B}(x,u) = \frac{2}{u}$, a constant selection

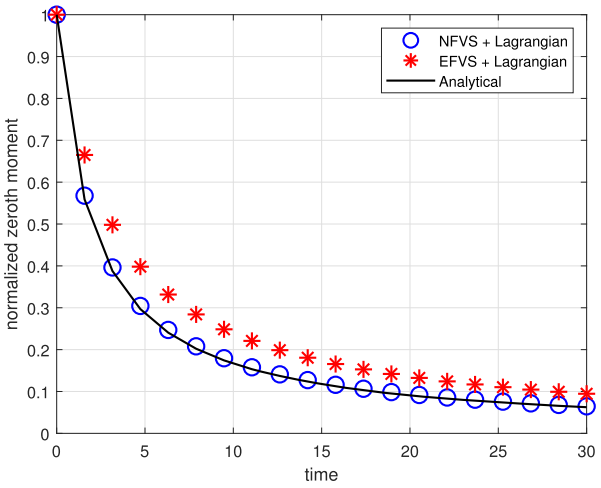

(a) Zeroth order moment

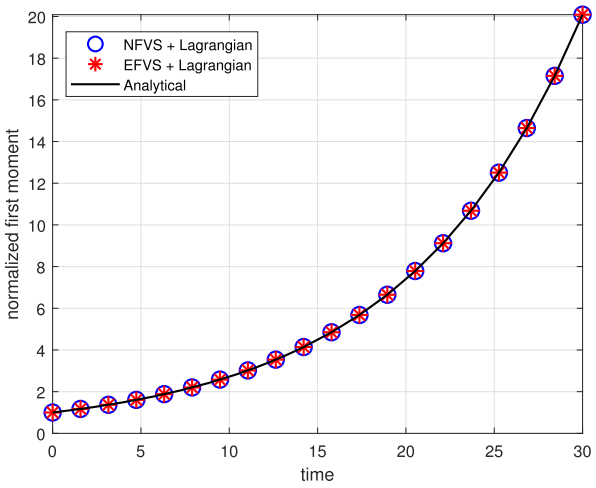

(b) First order moment

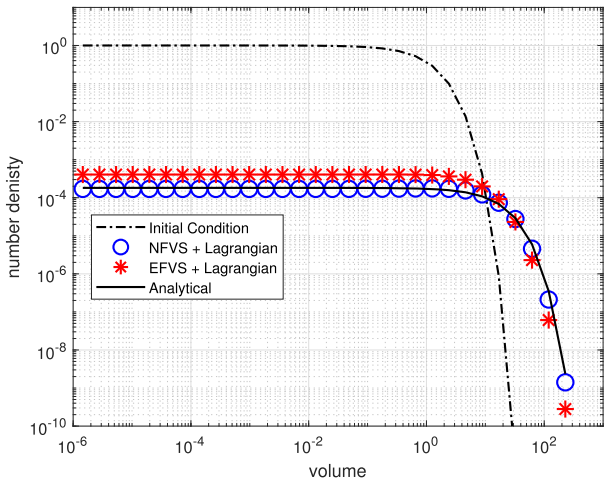

(c) Number density functions

Fig. 6 Testing of NFVS and EFVS of NDF and moments for Case 1; **a** zeroth order moment, **b** first order moment, and **c** number density function

Table 4 CPU time consumed (in seconds) by both FVS for Case 2

Constant kernel with linear growth			Sum kernel with linear growth		
Cells	Methods	CPU time	Cells	Methods	CPU time
30	NFVS	0.3786	30	NFVS	0.2151
30	EFVS	0.5033	30	EFVS	0.3449

function $F(x) = 1$, and a linear growth function $G(x) = G_0 x$ with $G_0 = 1$. The computational domain is defined as $[10^{-4}, 10]$, which is partitioned into 40 non-uniform cells. The simulations are conducted for a time period of $t = 0$ to $t = 3$. It is important to note that no analytical solutions of NDFs are available in the state of the art studies. However, Kumar et al. [31] provided mathematical expressions for the zeroth and first order moments for this specific case.

The numerical results in terms of moments and the NDF is qualitatively compared and shown in Fig. 8. As observed in previous cases, the NFVS demonstrates better accuracy in approximating the ZOM compared to the EFVS (refer to Fig. 8a). The proposed scheme accurately capture FOM as depicted in Fig. 8b whereas the existing scheme deviates from the exact result. Furthermore, the NDFs against the volume of a representation calculated numerically are plotted in Fig. 8c at different times (Table 5).

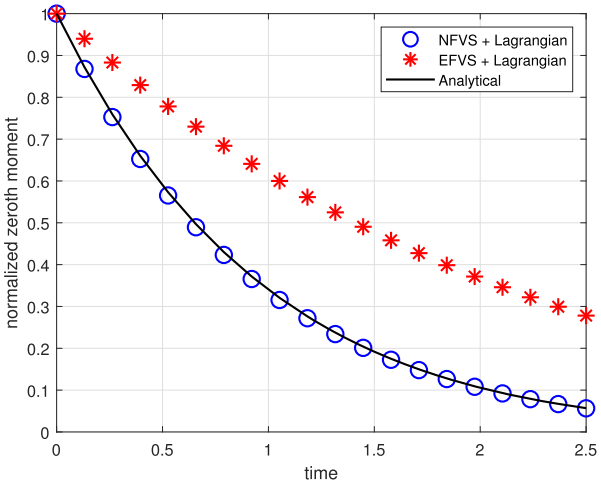

(a) Zeroth order moment

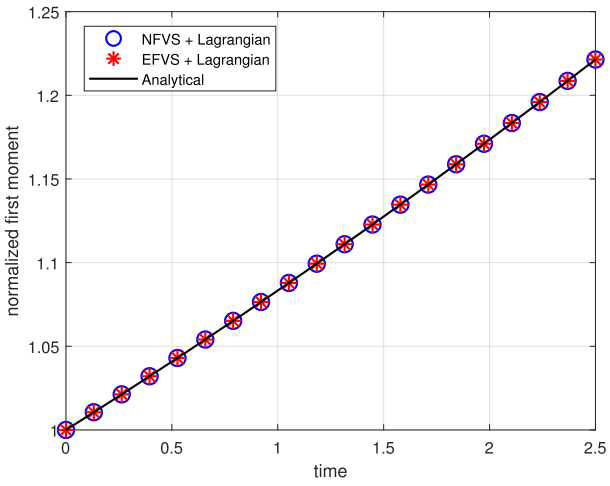

(b) First order moment

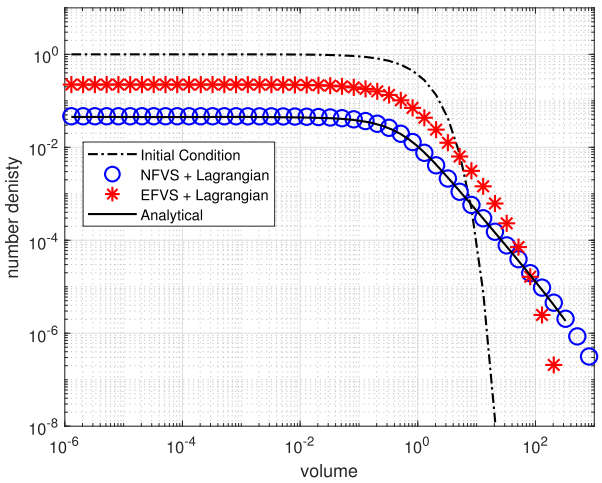

(c) NDFs

Fig. 7 Testing of NFVS and EFVS in terms of NDF and moments for Case 2; **a** zeroth order moment, **b** first order moment, and **c** number density function

Table 5 CPU time (in seconds) by numerical methods for simultaneous breakage-growth PBE

Method	Cells	CPU time	Cells	CPU time
NFVS	30	0.0115	60	0.0126
EFVS	30	0.0602	60	0.0633

3.5 Simultaneous aggregation-nucleation (SAN)

Now we compare the numerical results of the NFVS and EFVS for a SAN PBE by considering a $\alpha(x,u) = 1$ and an exponential nucleation function $Q_{nuc}(t,x) = \exp(-x)$ with $c = 1$ are considered. The numerical simulations are conducted on a computational domain of $[1\ \ 10^4]$ partitioned into 30 non-uniform grids. Both simulations are run until time $t = 10$. It is worth noting that Kumar et al. [52] have provided the exact solutions for both ZOM and FOM for this particular combination of aggregation kernel and nucleation function.

The comparison of results between the NFVS and EFVS for a SANPBE are shown in Fig. 9. It can be observed that the NFVS accurately approximates both ZOM and FOM, aligning closely with the reference solutions. On the other hand, the EFVS deviates from the exact moments as depicted in Fig. 9a and b. The NDFs obtained numerically are presented in Fig. 9c. Furthermore, the NFVS demonstrates better computational efficiency compared to the EFVS as indicated by the CPU times listed in Table 6.

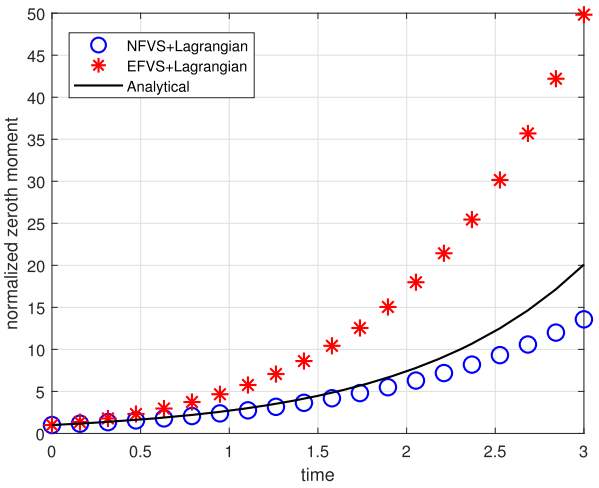

(a) Zeroth order moment

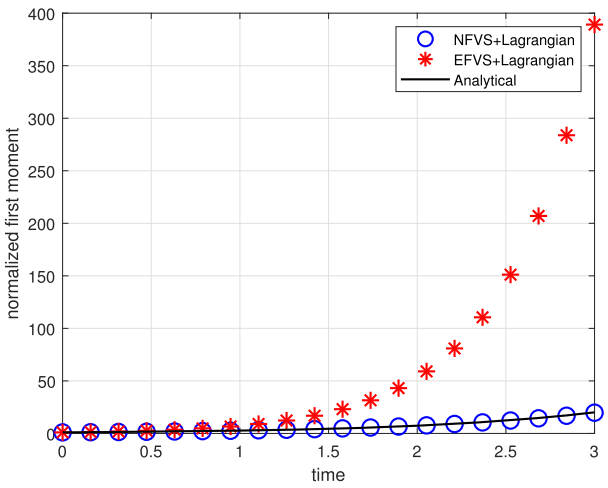

(b) First order moment

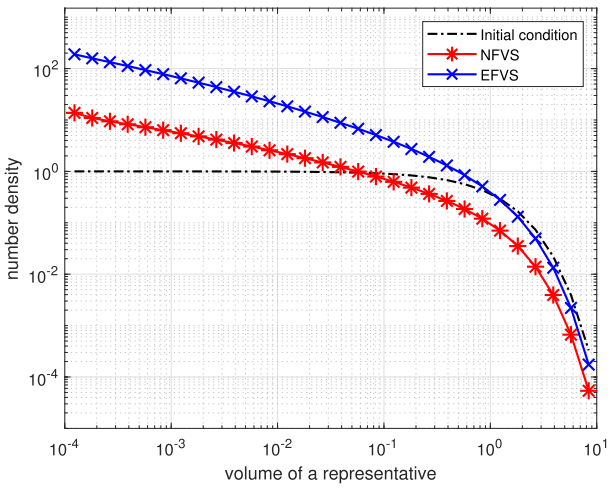

(c) NDFs

Fig. 8 Testing of NFVS and EFVS in terms of NDF and moments for binary breakage and linear growth functions **a** zeroth order moment, **b** first order moment, and **c** number density function

Table 6 CPU time consumed (in seconds) by numerical methods for SAN PBE

Method	Cells	CPU time	Cells	CPU time
NFVS	30	0.8986	45	1.2144
EFVS	30	3.4052	45	5.7995

3.6 Simultaneous breakage-nucleation (SBN)

Let us check the robustness of NFVS and EFVS with the exact solutions for a SBN PBE. The comparison is done using a binary breakage kernel $\mathcal{B}(x,u) = \frac{2}{u}$ and an exponential nucleation function $Q_{nuc}(t,x) = \exp(-cx)$, where $c = 1$. For this case no analytical (closed form) solutions for the NDF and moments are available. The computational domain $[10^{-4}, 10^{3}]$ is divided into 30 non-uniform cells, and the numerical results are estimated at time $t = 100$.

The ZOM and FOM are compared in Fig. 10a and b, respectively. It can be observed that the NFVS provides a more accurate prediction of the ZOM compared to the EFVS. However, NFVS also deviates, which can be improved by refining the grid and adding more cells. On the other hand, the EFVS fails to capture the FOM accurately, indicating its instability in approximating a simultaneous breakage-nucleation PBE. This highlights the challenges in solving superficially coupled processes.

The numerical results for the NDFs are qualitatively shown in Fig. 10c. It can be seen that the NFVS captures the trends of the NDFs reasonably well, while the EFVS exhibits

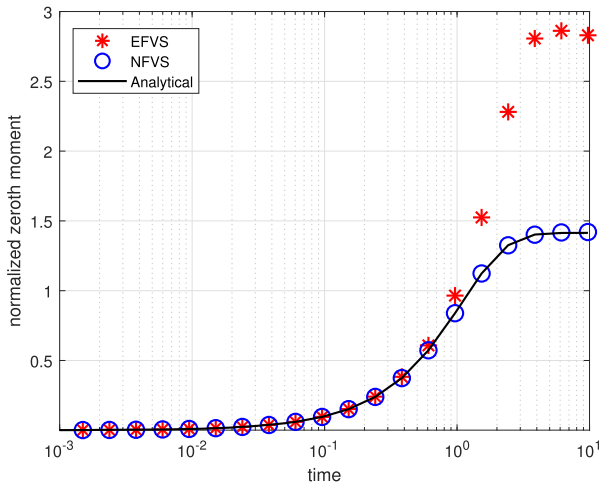

(a) Zeroth order moment

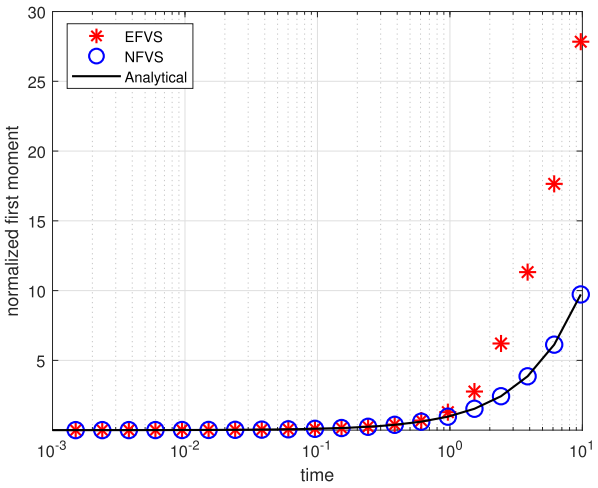

(b) First order moment

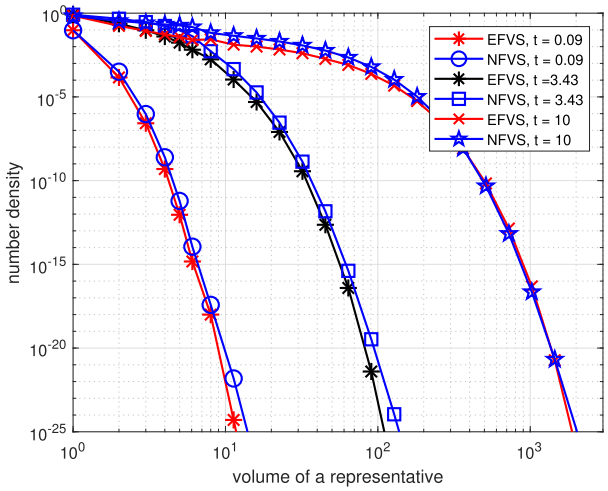

(c) NDFs

Fig. 9 Testing of NFVS and EFVS of NDF and moments for $\alpha(x, u) = 1$ and exponential nucleation function **a** zeroth order moment, **b** first order moment, and **c** number density function

Table 7 CPU time (in seconds) by numerical methods for SBN PBE

Method	Cells	CPU time	Cells	CPU time
NFVS	30	0.0115	60	0.0126
EFVS	30	0.0602	60	0.0633

significant deviations from the analytical result. Furthermore, in terms of CPU time, the NFVS outperforms the EFVS as shown in Table 7. This indicates that the NFVS is significant efficient in computing the results compared to the EFVS.

3.7 Simultaneous aggregation-breakage-growth (SABG)

To evaluate the performance of the NFVS and EFVS in a more complex system, we consider a scenario where aggregation, breakage, and growth processes are simultaneously affecting the particle properties. This scenario is commonly encountered in wet twin screw granulation and crystallization processes [71–73]. In this comparison, aggregation kernel $\alpha(x, u) = 1$ with $\mathcal{B}(x, u) = \frac{2}{u}$ and $F(x) = 1$ are used. The growth function is linear given by $G(x) = G_0 x$ with $G_0 = 0.1$.

The computational domain is set as $[10^{-6}\ \ 10^{5}]$ divided into 60 non-uniform cells. All numerical simulations are run until time $t = 2$. For this case also no closed-form solutions for the NDF are available. However, Kumar et al. [31] derived the exact results for the ZOM and FOM, which are used here for comparison.

The accuracy of the both approaches can be assessed by comparing the computed ZOM and FOM with the exact

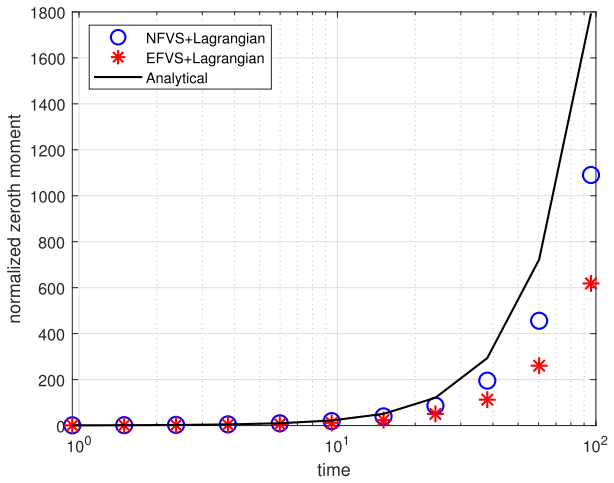

(a) Zeroth order moment

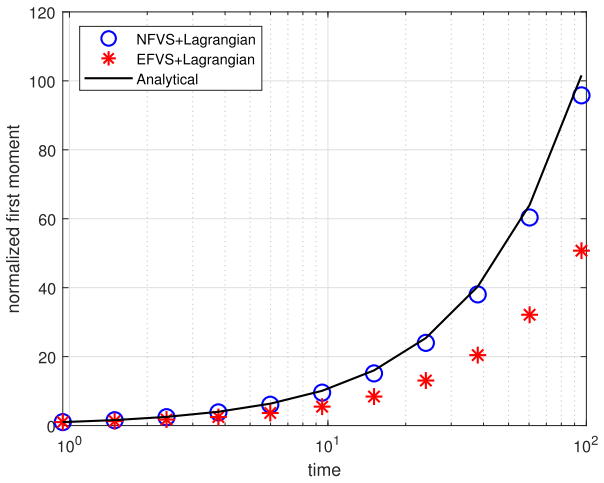

(b) First order moment

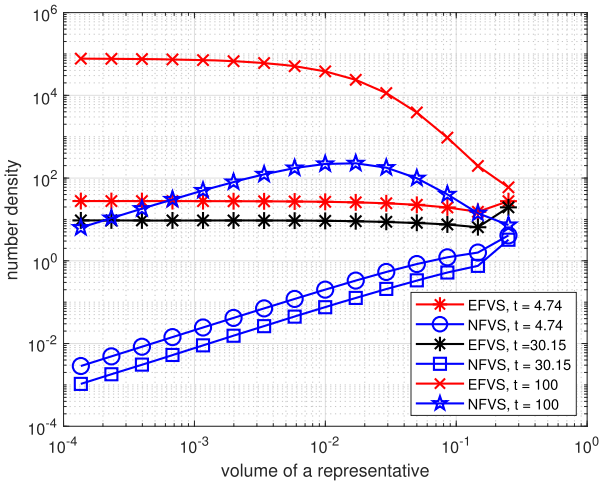

(c) NDFs

Fig. 10 Testing of NFVS and EFVS of NDF and moments for binary breakage kernel and exponential nucleation function **a** zeroth order moment, **b** first order moment, and **c** number density function

results. The numerical solutions for the NDFs are not directly compared due to the unavailability of analytical solutions. However, the moments can provide insights into the overall accuracy of the methods.

The comparison of the NDFs and its moments for this complex system is shown in Fig. 11. In the case of the NFVS, there is some deviation in computing the ZOM as depicted in Fig. 11a. This can be attributed to the fact that no specific measures were taken to estimate the ZOM accurately in this particular setup. However, the accuracy of the ZOM can be improved by using a more refined grid, although this may come at the expense of increased computational cost. On the other hand, the FOM, as shown in Fig. 11b, is very well captured by the NFVS. This indicates that the NFVS is capable of accurately estimating the total volume, which is an important property in many applications.

The numerical results for the NDFs as depicted in Fig. 11c, qualitatively. While we cannot directly compare these results with analytical solutions, they can still provide insights into the overall performance of the methods. In terms of efficiency, the NFVS took 4.6078 CPU time to estimate the numerical results with 30 non-uniform cells. This indicates that the NFVS is computationally efficient for this complex system.

Overall, the NFVS shows promising results in capturing the first order moment accurately and providing good estimates for the NDFs. The accuracy of the ZOM can be improved to a desired by refining the grid.

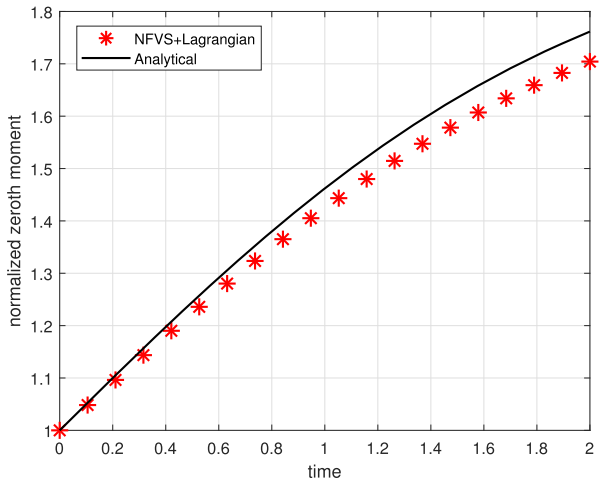

(a) Zeroth order moment

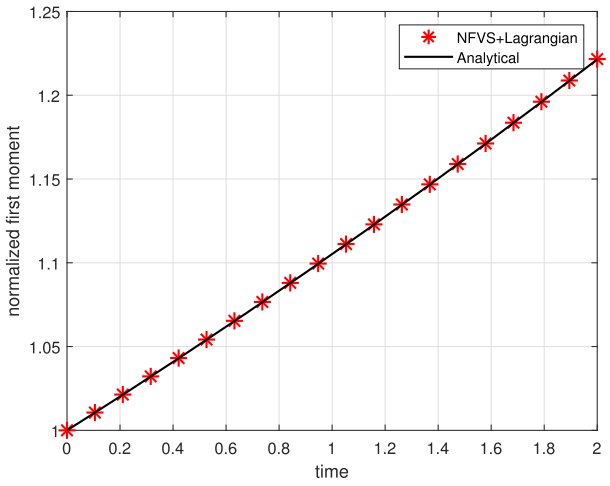

(b) First order moment

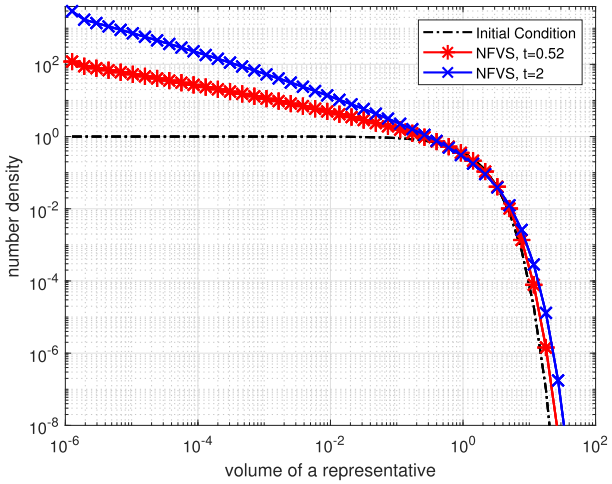

(c) NDFs

Fig. 11 Testing of NFVS of NDF and moments for SABG PBE **a** zeroth order moment, **b** first order moment, and **c** number density function

4 Concluding remarks and future prospects

In this study, we have developed new numerical methods to address the challenges associated with population balance models. For the first time, we present a comprehensive review of various numerical approaches for modelling aggregation, breakage, growth, and nucleation processes. To accurately capture the particle dynamics arising from growth and nucleation in the presence of aggregation and breakage, we employed a hybrid approach combining discrete finite volume schemes for the aggregation and breakage population balances with the method of characteristics. The source term associated with nucleation was positioned near the lower boundary of the first cell while simultaneously solving the coupled aggregation/breakage–nucleation equations.

It is worth noting that the existing finite volume scheme [29] exhibits significant deviations in approximating the zeroth order moments of the PBE. In some cases, the first order moment, which represents the total volume in the system, is also not accurately captured by their scheme. This highlights the limitations of the existing approach in accurately modelling and predicting the behaviour of the system. The proposed method has been thoroughly validated against analytical and existing numerical results, confirming its reliability and robustness. Overall, this work advances numerical modelling for population balances by providing a unified and efficient approach applicable to diverse chemical and phar-

maceutical processes, ultimately supporting deeper insights and optimization of complex particulate systems.

Author Contributions ZA: Conceptualization; Formal analysis; Investigation; Methodology; MATLAB coding; Validation; Writing—original draft; Writing-review and editing. MR: Formal analysis; Investigation; Methodology; Validation; Writing-review and editing. NS: Formal analysis; Investigation; Methodology; Validation; Writing-review and editing. MD: Formal analysis; Investigation; Methodology; Validation; Writing-review and editing. ST: Formal analysis; Investigation; Methodology; Validation; Writing-review and editing. SH: Formal analysis; Investigation; Methodology; Validation; Writing-review and editing. RR: Formal analysis; Investigation; Methodology; Validation; Writing-review and editing. GW: Formal analysis; Investigation; Methodology; Validation; Writing-review and editing. MS: Conceptualization; Formal analysis; Investigation; Methodology; Supervision; Validation; Writing—original draft; Writing-review and editing.

Funding Open Access funding provided by the IReL Consortium This publication has emanated from research funded by Research Ireland under grant numbers 18/CRT/6049 (Zeeshan Ansari). For the purpose of open access, the authors have applied a CC BY public copyright license to any Author Accepted Manuscript version arising from this submission.

Data Availability No new data were created or analysed in this study. Data sharing is not applicable to this article.

Declarations

Conflict of interest The author declares no conflict of interest.

References

1. Uppu A, Chaudhuri A, Das SP, Prakash N (2020) Cfd modeling of gypsum scaling in cross-flow ro filters using moments of particle population balance. J Environ Chem Eng 8(5):104151
2. Wang X, Cui B, Wei D, Song Z, He Y, Bayly AE (2021) Effect of feed solid concentration on tailings slurry flocculation in a thickener by a coupled cfd-pbm modelling approach. J Environ Chem Eng 9(6):106385
3. Hostomsky J, Jones AG (1991) Calcium carbonate crystallization, agglomeration and form during continuous precipitation from solution. J Phys D Appl Phys 24(2):165
4. Singh M, Walker G (2022) New discrete formulation for reduced population balance equation: an illustration to crystallization. Pharm Res 39(9):2049–2063
5. Ramkrishna D (2000) Population balances: theory and applications to particulate systems in engineering. Academic press
6. Singh M, Sriwastav N, Shardt O (2024) Efficient mass-preserving finite volume approach for the rennet-induced coagulation equation. Chaos Solitons Fract 181:114692
7. Ansari Z, Rae M, Singh M (2024) Two moments preserving sectional approach for an enzymatic coagulation equation. Phys Fluids 36(6):1–12
8. Ansari Z, Rae M, Kumar J, Singh M (2024) Optimizing numerical performance of enzymatic coagulation models: insight into proteolysis and gelation dynamics. Phys Fluids 36(11):117171
9. Sriwastav N, Das A, Shardt O, Kumar J, Singh M (2025) A meshfree approach for the rennet-induced coagulation equation: spline based multistage bernstein collocation method and its convergence analysis. Appl Math Model 143:116035
10. Kiparissides C (2006) Challenges in particulate polymerization reactor modeling and optimization: a population balance perspective. J Process Control 16(3):205–224
11. Peglow M, Kumar J, Mörl L (2005) Investigation of coalescence kinetics of microcristalline cellulose in fluidised bed spray agglomeration: experimental studies and modelling approach. Braz J Chem Eng 22(2):165–172
12. Barrasso D, Walia S, Ramachandran R (2013) Multi-component population balance modeling of continuous granulation processes: a parametric study and comparison with experimental trends. Powder Technol 241:85–97
13. Barrasso D, Eppinger T, Pereira FE, Aglave R, Debus K, Bermingham SK, Ramachandran R (2015) A multi-scale, mechanistic model of a wet granulation process using a novel bi-directional pbm-dem coupling algorithm. Chem Eng Sci 123:500–513
14. Ismail HY, Singh M, Shirazian S, Albadarin AB, Walker GM (2020) Development of high-performance hybrid ann-finite volume scheme (ann-fvs) for simulation of pharmaceutical continuous granulation. Chem Eng Res Des 163:320–326
15. Singh M, Shirazian S, Ranade V, Walker GM, Kumar A (2022) Challenges and opportunities in modelling wet granulation in pharmaceutical industry-a critical review. Powder Technol 2022:117380
16. Perry RH, Green DW (1999) Perry's chemical engineers' handbook. McGraw-Hill Professional
17. Ziff RM, McGrady ED (1986) Kinetics of polymer degradation. Macromolecules 19(10):2513–2519
18. Ziff RM (1991) New solutions to the fragmentation equation. J Phys A: Math Gen 24(12):2821
19. Leyvraz F (2003) Scaling theory and exactly solved models in the kinetics of irreversible aggregation. Phys Rep 383(2–3):95–212
20. Ziff RM (1992) An explicit solution to a discrete fragmentation model. J Phys A: Math Gen 25(9):2569
21. Yadav N, Singh M, Singh S, Singh R, Kumar J (2023) A note on homotopy perturbation approach for nonlinear coagulation equation to improve series solutions for longer times. Chaos Solitons Fract 173:113628
22. Yadav N, Das A, Singh M, Singh S, Kumar J (2023) Homotopy perturbation method and its convergence analysis for nonlinear collisional fragmentation equations. Proc R Soc A 479(2279):20230567
23. Yadav S, Keshav S, Singh S, Singh M, Kumar J (2023) Homotopy analysis method and its convergence analysis for a nonlinear simultaneous aggregation-fragmentation model. Chaos Solitons Fract 177:114204
24. Yadav N, Ansari Z, Singh R, Das A, Singh S, Heinrich S, Singh M (2024) Explicit and approximate solutions for a classical hyperbolic fragmentation equation using a hybrid projected differential transform method. Phys Fluids 36(9):093343
25. Yadav S, Das A, Singh S, Tomar S, Singh R, Singh M (2024) Coupled approach and its convergence analysis for aggregation and

breakage models: study of extended temporal behaviour. Powder Technol 439:119714
26. Yadav S, Singh M, Singh S, Heinrich S, Kumar J (2024) Modified variational iteration method and its convergence analysis for solving nonlinear aggregation population balance equation. Comput Fluids 274:106233
27. Yadav N, Singh M, Singh S, Singh R, Kumar J, Heinrich S (2024) An efficient approach to obtain analytical solution of nonlinear particle aggregation equation for longer time domains. Adv Powder Technol 35(3):104370
28. Bourgade J-P, Filbet F (2008) Convergence of a finite volume scheme for coagulation-fragmentation equations. Math Comput 77(262):851–882
29. Qamar S, Warnecke G, Elsner MP (2009) On the solution of population balances for nucleation, growth, aggregation and breakage processes. Chem Eng Sci 64(9):2088–2095
30. Kumar R, Kumar J (2013) Numerical simulation and convergence analysis of a finite volume scheme for solving general breakage population balance equations. Appl Math Comput 219(10):5140–5151
31. Kumar R, Kumar J, Warnecke G (2013) Moment preserving finite volume schemes for solving population balance equations incorporating aggregation, breakage, growth and source terms. Math Models Methods Appl Sci 23(07):1235–1273
32. Singh M, Ismail HY, Matsoukas T, Albadarin AB, Walker G (2019) Mass-based finite volume scheme for aggregation, growth and nucleation population balance equation. Proc R Soc A 475(2231):20190552
33. Singh M, Matsoukas T, Albadarin AB, Walker G (2019) New volume consistent approximation for binary breakage population balance equation and its convergence analysis. ESAIM Math Model Numer Anal 53(5):1695–1713
34. Singh M, Matsoukas T, Walker G (2020) Mathematical analysis of finite volume preserving scheme for nonlinear smoluchowski equation. Phys D 402:132221
35. Singh M (2023) Rate of convergence of two moments consistent finite volume scheme for non-classical divergence coagulation equation. Appl Numer Math 187:120–137
36. Marchisio DL, Pikturna JT, Fox RO, Dennis Vigil R, Barresi AA (2003) Quadrature method of moments for population-balance equations. AIChE J 49(5):1266–1276
37. Yuan C, Laurent F, Fox RO (2012) An extended quadrature method of moments for population balance equations. J Aerosol Sci 51:1–23
38. Laurent TTNF, Fox RO, Massot M (2016) Solution of population balance equations in applications with fine particles: mathematical modeling and numerical schemes. J Comput Phys 325:129–156
39. Pigou M, Morchain J, Fede P, Penet M-I, Laronze G (2018) New developments of the extended quadrature method of moments to solve population balance equations. J Comput Phys 365:243–268
40. Pütz M, Pollack M, Hasse C, Oevermann M (2022) A gauss/anti-gauss quadrature method of moments applied to population balance equations with turbulence-induced nonlinear phase-space diffusion. J Comput Phys 466:111363
41. Kumar S, Ramkrishna D (1997) On the solution of population balance equations by discretization-iii. nucleation, growth and aggregation of particles. Chem Eng Sci 52(24):4659–4679
42. Vale HM, McKenna TF (2005) Solution of the population balance equation for two-component aggregation by an extended fixed pivot technique. Ind Eng Chem Res 44(20):7885–7891
43. Nandanwar MN, Kumar S (2008) A new discretization of space for the solution of multi-dimensional population balance equations: simultaneous breakup and aggregation of particles. Chem Eng Sci 63(15):3988–3997
44. Chauhan SS, Chiney A, Kumar S (2012) On the solution of bivariate population balance equations for aggregation: X-discretization of space for expansion and contraction of computational domain. Chem Eng Sci 70:135–145
45. Saha J, Singh M (2023) Rate of convergence and stability analysis of a modified fixed pivot technique for a fragmentation equation. Numer Math 153(2):531–555
46. Zuwei X, Zhao H, Zheng C (2015) Accelerating population balance-monte carlo simulation for coagulation dynamics from the markov jump model, stochastic algorithm and gpu parallel computing. J Comput Phys 281:844–863
47. Patterson RIA, Wagner W, Kraft M (2011) Stochastic weighted particle methods for population balance equations. J Comput Phys 230(19):7456–7472
48. Lee KF, Patterson RIA, Wagner W, Kraft M (2015) Stochastic weighted particle methods for population balance equations with coagulation, fragmentation and spatial inhomogeneity. J Comput Phys 303:1–18
49. Haibo Zhao F, Kruis E, Zheng C (2010) A differentially weighted monte carlo method for two-component coagulation. J Comput Phys 229(19):6931–6945
50. Zhao H, Zheng C (2013) A population balance-monte carlo method for particle coagulation in spatially inhomogeneous systems. Comput Fluids 71:196–207
51. Kotalczyk G, Einar Kruis F (2017) A monte carlo method for the simulation of coagulation and nucleation based on weighted particles and the concepts of stochastic resolution and merging. J Comput Phys 340:276–296
52. Kumar J, Peglow M, Warnecke G, Heinrich S (2008) An efficient numerical technique for solving population balance equation involving aggregation, breakage, growth and nucleation. Powder Technol 182(1):81–104
53. Mehakpreet Singh G, Kaur JK, De Beer T, Nopens I (2018) A comparative study of numerical approximations for solving the smoluchowski coagulation equation. Braz J Chem Eng 35(4):1343–1354
54. Singh M, Kumar A, Shirazian S, Ranade V, Walker G (2020) Characterization of simultaneous evolution of size and composition distributions using generalized aggregation population balance equation. Pharmaceutics 12(12):1152
55. Singh M (2021) New finite volume approach for multidimensional smoluchowski equation on nonuniform grids. Stud Appl Math 147(3):955–977
56. Singh M, Matsoukas T, Walker G (2021) Two moments consistent discrete formulation for binary breakage population balance equation and its convergence. Appl Numer Math 166:76–91
57. Singh M, Walker G (2022) Finite volume approach for fragmentation equation and its mathematical analysis. Numer Algorithms 89(2):465–486
58. Kumar S, Ramkrishna D (1996) On the solution of population balance equations by discretization-I. a fixed pivot technique. Chem Eng Sci 51(8):1311–1332
59. Singh M, Ranade V, Shardt O, Matsoukas T (2022) Challenges and opportunities concerning numerical solutions for population balances: a critical review. J Phys A: Math Theor 55(38):383002
60. Hong Z, Long Y, Lian B, Shan B, Qilei X, Wang Y, Wang XZ, Zhang F (2024) Improved high-resolution algorithm for solving population balance equations. Ind Eng Chem Res 63(12):5339–5356
61. Zhang W, Przybycien T, Schmölder J, Leweke S, von Lieres E (2024) Solving crystallization/precipitation population balance models in cadet, part i: nucleation growth and growth rate dispersion in batch and continuous modes on nonuniform grids. Comput Chem Eng 183:108612
62. Inguva PK, Braatz RD (2023) Efficient numerical schemes for multidimensional population balance models. Comput Chem Eng 170:108095
63. Zhang F, Hong Z, Li C, Diao Z, Lian B, Shan B, Wang Y, Qilei X (2025) High-order compact difference method for solving popula-

tion balance equations in batch crystallization. Ind Eng Chem Res 64(6):3568–3577
64. Filbet F, Laurençot P (2004) Numerical simulation of the smoluchowski coagulation equation. SIAM J Sci Comput 25(6):2004–2028
65. Singh M, Kumar J, Bück A, Tsotsas E (2015) A volume-consistent discrete formulation of aggregation population balance equations. Math Methods Appl Sci 39(9):2275–2286
66. Saha J, Kumar J (2015) Development of a mass conserving discretization technique for breakage problems and its convergence analysis. Int J Adv Eng Sci Appl Math 7(1–2):51–61
67. Singh M (2021) Accurate and efficient approximations for generalized population balances incorporating coagulation and fragmentation. J Comput Phys 435:110215
68. Kumar J, Peglow M, Warnecke G, Heinrich S (2008) An efficient numerical technique for solving population balance equation involving aggregation, breakage, growth and nucleation. Powder Technol 182(1):81–104
69. Qamar S, Warnecke G (2007) Numerical solution of population balance equations for nucleation, growth and aggregation processes. Comput Chem Eng 31(12):1576–1589
70. Hu Q, Rohani S, Jutan A (2005) New numerical method for solving the dynamic population balance equations. AIChE J 51(11):3000–3006
71. Chaudhury A, Huiquan W, Khan M, Ramachandran R (2014) A mechanistic population balance model for granulation processes: effect of process and formulation parameters. Chem Eng Sci 107:76–92
72. Chaudhury A, Armenante ME, Ramachandran R (2015) Compartment based population balance modeling of a high shear wet granulation process using data analytics. Chem Eng Res Des 95:211–228
73. Ismail HY, Shirazian S, Singh M, Whitaker D, Albadarin AB, Walker GM (2020) Compartmental approach for modelling twin-screw granulation using population balances. Int J Pharm 576:118737